

Analytical cell size distribution: lineage-population bias and parameter inference

Arthur Genthon

*Gulliver UMR CNRS 7083, ESPCI Paris, Université PSL, 75005 Paris, France**

Solving population balance equations, we derive analytical steady-state cell size distributions for single-lineage experiments, such as the mother machine. These experiments are fundamentally different from batch cultures where populations of cells grow freely, and the statistical bias between them is obtained by comparing our results to cell size distributions measured in population. For exponential single-cell growth, characterizing most bacteria, the lineage-population bias is obtained explicitly. In addition, if volume is evenly split between the daughter cells at division, we show that cells are on average smaller in populations. For more general power-law growth rates and deterministic volume partitioning, both symmetric and asymmetric, we derive the exact lineage distribution. This solution is in good agreement with *E. Coli* mother machine data, and can be used to infer cell cycle parameters, such as the strength of the size control and the asymmetry of the division. When introducing stochastic volume partitioning, we derive the large-size and small-size tails of the lineage size distributions, and show that they respectively do not depend on the partitioning of volume and on the size control strength. Finally, we show that introducing noise, either on the volume partitioning or on the single cell growth rate, can cancel the lineage-population bias.

I. INTRODUCTION

In the past decade, a large amount of single-cell data has been obtained thanks to microfluidic devices, such as the mother machine [1]. In these experiments, time-lapse video-microscopy allows to follow single-cell lineages over many generations with great precision, resulting in large and reliable statistics. Several questions are then naturally raised: How can we use these data to infer the laws of cell growth and division? Can we learn population-level properties from single-lineage measurements? Are single-lineage statistics different from population statistics obtained in batch cultures?

The first two questions received recent attention. For example, Jia et al. proposed a method to infer single-cell parameters from size distributions, both for bacteria [2] and yeasts [3]. Also, single-lineage statistics on the number of divisions can in principle be used to estimate the population growth rate, with which the population would grow in a batch culture [4–6].

The answer to the third question is yes, and quantifying the differences between these two perspectives is fundamental in order to compare and analyze the different sets of data. This problem can be traced back to Powell's 1956 seminal work [7], in which he showed that for age-structured populations in exponential growth, the lineage and population distributions of generation times (time elapsed between birth and division) are different. This difference is understood as cells that divided more than average lead to subpopulations of offsprings that are over-represented in the population, while no such selection is present in single-lineage experiments. Powell's results have been generalized in several directions since [5, 8, 9]. The problem was recently reformulated by Nozoe et al. [10] in terms of two different samplings of lineages in a population tree, and their framework has been used to further investigate the lineage-population bias [11, 12], its consequences on selection strength [13], and has been analyzed through the lens of stochastic thermodynamics [5, 14]. The lineage-population bias for any cell trait can be studied using the notion of fitness landscape [10], which quantifies the correlations between the value of the trait and the number of divisions undergone by the cell. We showed in some simple cases that for age and size, the population distributions of these traits are biased toward small values as compared to the lineage statistics [5], because cells that divided a lot are on average smaller and younger. Another route to investigate this bias, that we take in this article, is to solve independently the population and lineage equations.

In this article, we focus on cell size which offers many insights on the laws of growth and division, and because the size framework also applies to molecular-level quantities, such as a number of proteins or mRNA, which also grow within the cell cycle and are split between the daughter cells at division. Lineage-population biases have been recently derived at the level of the first moments of the size distribution [15], and of the distribution of size at birth [12] in some particular cases; however general understanding of the bias at the level of distributions, as illustrated on fig. 1, is lacking. In the mathematical literature, the growth-fragmentation equation modeling the time evolution of the

* arthur.genthon@espci.fr

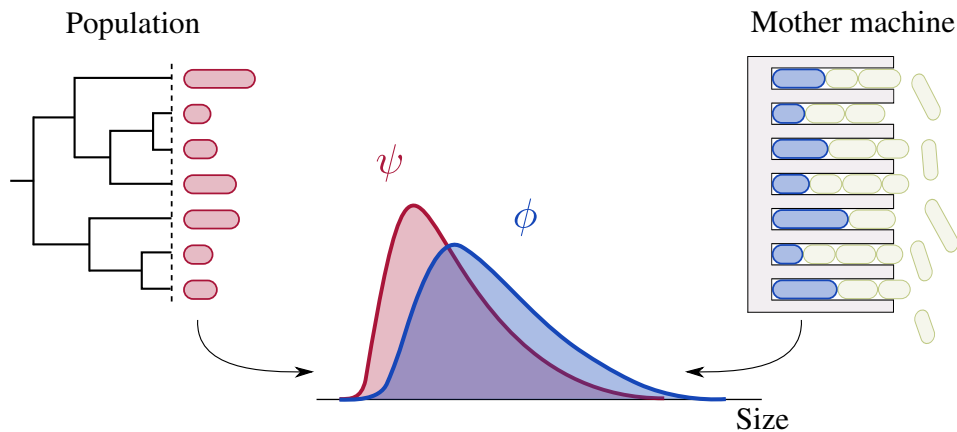


Figure 1. Snapshot cell-size distributions for two different experimental setups. The population distribution ψ (red) is computed by uniformly sampling cell sizes in a freely growing population in a batch culture, and the lineage distribution ϕ (blue) is obtained by uniformly sampling the sizes of the constant number of mother cells (in blue) at the bottoms of each micro-channel in a mother machine device.

population cell-size distribution has been largely analyzed [16–18]. Surprisingly, these analyses have not been applied to lineage statistics.

The fluctuations in cell growth are of central importance for cell size statistics. Variability in single cell growth has been mainly modeled as a Markov process, where the single cell growth rate changes from one cycle to the next one, but remains constant inside each cycle, so that the growth of a single cell is deterministic [14, 19]. This kind of modeling accounts for cell-to-cell variability, which affects the population growth rate [20], either increasing or decreasing it depending on mother-daughter correlations [21]. On the other hand, experimental cycles exhibit fluctuations around the exponential trend, prompting us to describe single-cell growth as a random process with a diffusive term accounting for in-cycle variability. Experimental data on *E. Coli* [22] suggest that both in-cycle and cell-to-cell sources of variability are present. However, numerical results show that the cell-to-cell variability in growth has little impact on the steady-state size distribution [2]. We thus decide to focus on the in-cycle source of variability in cell growth.

The goals of this article are multiple and are summarized as follows. After introducing the model in section II, we derive in section III exact steady-state lineage cell-size distributions, in the case of deterministic volume partitioning, both symmetric and asymmetric. The lineage-population bias is then obtained by comparison with the mathematical literature on population. We also show that this result accounts for experimental data, and can be used for parameters inference. In section IV, we introduce stochasticity in the partitioning and seek large and small size asymptotic lineage distributions, from which the lineage-population bias is derived. In section V, we introduce in-cycle noise around exponential growth, and show how it modifies the large-size behavior and the lineage-population bias.

II. PRELIMINARIES

A. Model and definitions

The number $n(x, t)$ of cells of size x at time t obeys the following population balance equation (PBE):

$$\partial_t n(x, t) = -\partial_x[\nu(x)n(x, t)] + \partial_{x^2}[D(x)n(x, t)] - r(x)n(x, t) + m \int \frac{dx'}{x'} b(x/x') r(x') n(x', t), \quad (1)$$

supplemented with the ‘no-flux’ boundary conditions at $x = 0$ and $x = \infty$:

$$\begin{aligned} 0 &= \lim_{x \rightarrow 0} \partial_x [D(x)n(x, t)] - \nu(x)n(x, t) \\ &= \lim_{x \rightarrow \infty} \partial_x [D(x)n(x, t)] - \nu(x)n(x, t), \end{aligned} \quad (2)$$

and the initial condition $n(x, t = 0) = n_0(x)$. In the right hand side, the first two terms account respectively for the deterministic part of the cell growth with rate $\nu(x)$, and for the stochastic part of the growth where $D(x)$ is the diffusion coefficient. In the corresponding Langevin representation of the cell cycle, size grows as $dx = \nu(x)dt + \sqrt{2D(x)}dW$

where W is the Wiener process. The third term describes the division of cells of size x with a rate $r(x)$, and the last term accounts for the birth of m new cells of size x coming from the divisions of cells of sizes x' , through the partition kernel $b(x/x')$ which is the probability for a newborn cell to inherit the fraction x/x' of its mother's volume at division. Most cells obey *binary fission* corresponding to $m = 2$. The partition kernel is normalized as $\int_0^1 dx b(x) = 1$, and the conservation of volume at division imposes that $m \int_0^1 dx xb(x) = 1$. Moreover, births of cells of size 0 are impossible, so that we set $b(0) = b(1) = 0$. The kernel b is very general, and accounts for *deterministic symmetric partition* observed in bacteria and fission yeast: $b(x) = \delta(x - 1/m)$; *deterministic asymmetric partition* characterizing for example budding yeast: $b(x) = \sum_{i=1}^m \delta(x - 1/\omega_i)/m$ with $\omega_i > 1$ and $\sum_{i=1}^m 1/\omega_i = 1$; and *stochastic partition* which can be modeled for example as a Beta distribution for size or as a Binomial distribution for protein segregation.

We recast this equation at the probability level by defining the frequency $\psi(x, t) = n(x, t)/N_t$ of cells of size x , with $N_t = \int dx n(x, t)$ the total number of cells at time t :

$$\partial_t \psi(x, t) = -\partial_x [\nu(x)\psi(x, t)] + \partial_{x^2} [D(x)\psi(x, t)] - [r(x) + \Lambda_t] \psi(x, t) + m \int \frac{dx'}{x'} b(x/x') r(x') \psi(x', t), \quad (3)$$

where $\Lambda_t = \partial_t N_t / N_t$ is the instantaneous population growth rate. Direct integration of this equation with respect to x shows that this population growth rate is equal to the average division rate:

$$\Lambda_t = (m - 1) \int dx r(x) \psi(x, t). \quad (4)$$

We refer to this distribution ψ as the population distribution, and draw the attention of the reader on the fact that adding a uniform (x -independent) death/dilution rate does not affect this population distribution [8, 23]. In particular, setting a dilution rate that perfectly balances the population growth allows to maintain constant populations, as it is done in chemostats, but does not affect the size-distribution.

The equation for the lineage distribution $\phi(x)$ is obtained from eq. (3) by tracking only $m = 1$ daughter cell at division [24], thus maintaining the population constant with a null growth rate Λ_t :

$$\partial_t \phi(x, t) = -\partial_x [\nu(x)\phi(x, t)] + \partial_{x^2} [D(x)\phi(x, t)] - r(x)\phi(x, t) + \int \frac{dx'}{x'} b(x/x') r(x') \phi(x', t). \quad (5)$$

Importantly, we set $m = 1$ without changing the partition kernel: even though we follow only one of the m daughters at division, it still inherits $1/m$ of the mother volume (for symmetric partitioning) and not 1. In this sense, this equation is not equivalent to the one obtained in the limit $m \rightarrow 1^+$ considered in [25]. Note that, if the lineage distribution is defined as a snapshot distribution, it can be evaluated along a single lineage in time because of the ergodic principle.

In the following, we focus on power-law division and growth rates:

$$r(x) = rx^\alpha \quad (6)$$

$$\nu(x) = \nu x^\beta. \quad (7)$$

This choice for the division rate can be justified theoretically [26] and the power α is the strength of the size-control: in the limit $\alpha \rightarrow 0$ of weak control, cells of all sizes divide with the same rate, while in the limit $\alpha \rightarrow +\infty$ of strong control, cells divide deterministically when reaching size $x = 1$. The power law for the growth rate includes the most common growth strategies, which we call *linear growth* for $\beta = 0$, and *exponential growth* which characterizes most bacteria [27] for $\beta = 1$.

In the long-time limit the population grows exponentially with a rate $\Lambda = \lim_{t \rightarrow \infty} \Lambda_t$ and reaches steady-state size distributions, if certain conditions are met [16–18]. Among them, $\alpha - \beta + 1 > 0$ ensures that there is enough division to avoid cells of diverging sizes, and that there is enough growth to avoid cells of vanishing sizes. Additionally, for partitioning kernels such as $b(x) \underset{x \rightarrow 0}{\sim} b_0 x^{\gamma_0}$ that allow births of cells with vanishing volumes, the condition $\gamma_0 > \beta$ guarantees that there is enough growth to counterbalance birth. In this article, we suppose that these conditions are fulfilled.

Through the article we use moments of order k of the distributions b , ψ and ϕ , which are the Mellin transforms of

these distributions (up to a constant 1 in the exponent):

$$L_k = \int_0^1 x^k b(x) dx \quad (8)$$

$$M_k = \int_0^\infty x^k \psi(x) dx \quad (9)$$

$$N_k = \int_0^\infty x^k \phi(x) dx. \quad (10)$$

B. The special case of exponential growth

When cells grow exponentially with a rate $\nu(x) = \nu x$, two important results are derived.

First, the steady-state population growth matches the single cell growth rate [28]. This follows from the integration of eq. (3) after multiplication by x , and using the mass conservation property of kernel b :

$$\partial_t M_1 = (\nu - \Lambda_t) M_1, \quad (11)$$

where M_1 is the average size in the population statistics. Therefore, in steady-state the left hand side is null and $\Lambda_t \equiv \Lambda = \nu$.

Second, the lineage-population bias takes a very simple form. In the absence of noise, the Langevin dynamics of cell growth is given by $dx = \nu x dt$, and when considering noisy exponential growth, a Gaussian noise is put on the growth rate itself [29]: $dx = (\nu dt + \sqrt{2D} dW)x$, leading to a diffusion coefficient $D(x) = D x^2$ in eq. (1), which we call *multiplicative noise*. We show in appendix A that the steady-state population distribution $\psi_\nu^{b(x)}$ for growth rate ν and partition kernel $b(x)$ is equal to the lineage distribution $\phi_{\nu+2D}^{mxb(x)}$ for the modified dynamics $\hat{\nu} = \nu + 2D$ and $\hat{b}(x) = mxb(x)$, divided by the size:

$$\phi_{\nu+2D}^{mxb(x)}(x) = K x \psi_\nu^{b(x)}(x), \quad (12)$$

where $K = \left(\int_0^\infty dx x \psi_\nu^{b(x)}(x) \right)^{-1}$ is a normalization constant. In the case of deterministic symmetric partitioning, the modified partition kernel $\hat{b}(x) = mxb(x) = mx\delta(x - 1/m) = \delta(x - 1/m) = b(x)$ in the single lineage dynamics is equal to the partition kernel $b(x)$ in the population dynamics. Note that this is not true for deterministic asymmetric partitioning. In addition, if there is no noise on the growth, that is when $D = 0$, then we recover $\phi(x) = Kx\psi(x)$ [30].

From this relation, it is straightforward to show that

$$\begin{aligned} \int_0^\infty dx x \phi(x) &= N_1 = M_1 + \frac{M_2 - M_1^2}{M_1} \\ &\geq M_1 = \int_0^\infty dx x \psi(x), \end{aligned} \quad (13)$$

where the inequality comes from the positivity of the variance $M_2 - M_1^2$ of the size in the population dynamics. Therefore, the average size is larger in lineages than in populations.

A parallel can be drawn between eq. (12) and the bias derived using the notion of fitness landscape for a branching tree starting with an ancestor cell of size x_0 [5]. We obtained a lineage-population bias involving a factor x , which comes from the correlations between the size x at time t and the number of divisions in the lineage of the cell up to time t . Although the frameworks are different, we think that the origin of the factor x in eq. (12) is also due to these correlations. Moreover, it is clear that if no such correlations are present, the over-representation of lineages with high-reproductive success in a population does not affect the size distribution, so that the lineage and population size distributions are identical.

III. EXACT LINEAGE DISTRIBUTIONS FOR DETERMINISTIC PARTITIONING

Exact population solutions to eq. (3) have been obtained in the particular case of exponential and noiseless ($D = 0$) growth, for deterministic symmetric [28] and asymmetric [31] partitioning. The same methods can be used to derive the lineage distribution, for which the hypothesis of exponential growth can even be relaxed and replaced by power-law growth rates, still in the absence of noise.

For symmetric partitioning between the m daughter cells, we show in appendix B 1 that the solution reads

$$\phi(x) = \frac{C}{x^\beta} \sum_{k=0}^{\infty} c_k \exp \left[-m^{k(\alpha-\beta+1)} \frac{r}{\nu} \frac{x^{\alpha-\beta+1}}{\alpha-\beta+1} \right], \quad (14)$$

where the coefficients c_k are given in appendix B 1 and C is a normalization constant. For exponential growth, we find that this lineage distribution is related to the population distribution $\psi(x)$ obtained in [28] by $\phi(x) = x\psi(x)$, which was expected in the light of section II B.

It is worth mentioning that this distribution takes a very simple form in the limit of strong control $\alpha \rightarrow +\infty$, where cells divide deterministically when reaching size 1. In this limit, $c_0 = 1$, c_1 tends to -1 and all other c_k tend to 0, such that the lineage size distribution reduces to $\phi(x) = Cx^{-\beta}$ for $x \in [1/m, 1]$ and 0 otherwise. This result is analogous to the one for populations: $\psi(x) \propto x^{-2}$ for $x \in [1/2, 1]$ and 0 otherwise, obtained for binary fission and exponential growth [12, 28]. Note also that in this limit, there is no randomness in the dynamics of cell growth and division, and thus the steady-state size distribution is simply the solution to the flux-balance equation $\partial_x[\nu(x)\phi(x, t)] = 0$.

In the case of asymmetric partitioning, for simplicity we choose to focus on binary fission. The volume of the dividing cell is split unequally between the daughters: one inherits a fraction $1/\omega_1$ of the mother size and the other daughter a fraction $1/\omega_2$, with $\omega_1 > \omega_2 > 1$ and $1/\omega_1 + 1/\omega_2 = 1$. The choice of the protocol to track one of the two daughters is of major importance [2]. If one chooses to always track the smallest of the two daughters, then the partition kernel is given by: $b(x) = \delta(x - 1/\omega_1)$. This is equivalent to the partition kernel for symmetric partitioning between m daughter cells where m is replaced by ω_1 , and the size distribution is therefore given by eq. (14), when replacing m by ω_1 . On the other hand, in the random tracking protocol, each cell is tracked at division with probability $1/2$, so that the partition kernel is given by $b(x) = \delta(x - 1/\omega_1)/2 + \delta(x - 1/\omega_2)/2$. In this case, we show in appendix B 2 that the size distribution reads

$$\phi(x) = \frac{C}{x^\beta} \sum_{k=0}^{\infty} \sum_{l=0}^{\infty} c_{k,l} \exp \left[-\omega_1^{k(\alpha-\beta+1)} \omega_2^{l(\alpha-\beta+1)} \frac{r}{\nu} \frac{x^{\alpha-\beta+1}}{\alpha-\beta+1} \right], \quad (15)$$

where the coefficients $c_{k,l}$ are given in appendix B 2 and C is a normalization constant. For exponential growth, we find that this lineage distribution is related to the population distribution $\psi(x)$ obtained in [31] by $\phi^{2xb(x)}(x) = x\psi^{b(x)}(x)$, which we expected in the light of section II B. Note that unlike what happens for symmetric partitioning, the coefficients $c_{k,l}$ appearing in the lineage and population distributions are different because the biased partition kernel $2xb(x)$ is different from $b(x)$.

A. Shapes of the theoretical solutions

We numerically investigate the influence of the parameters of the model on the analytical steady-state size distributions eq. (14) and eq. (15), and show the results on fig. 2. The first row corresponds to symmetric partitioning and the second one to asymmetric partitioning. On the top left plot, as the strength of the size control α is increased the distribution gets narrower, and in the limit of large control, division becomes deterministic and $\phi(x) = Cx^{-\beta}$ for $x \in [1/2, 1]$. On the top right plot, the growth rate power β is varied. For $\beta = 0$, ϕ presents a flat maximum and a fast decline for large size. As β increases, the maximum becomes more peaked and the decrease at large size is slowed, which follows from the fact that increasing the growth rate allows cells to reach larger sizes. On the bottom left plot, we vary the volume ratio $1/\omega_1$ of the cell that we follow at each division. The smaller the daughter we follow, the wider the curve on the left hand side. Finally, the bottom right plot corresponds to the random tracking protocol, where $1/\omega_1$ is the ratio of the smallest of the two daughters cells. As the asymmetry is increased, the curve becomes bimodal, intuitively corresponding to the two subpopulations produced by the smaller and larger daughters at each division. Note that for this protocol, we chose values of $1/\omega_1$ below 0.5 only, because the conservation of volumes imposes that distributions are identical for values of $1/\omega_1$ symmetrical around 0.5.

B. Test on experimental data: parameters inference

In experimental systems, the partitioning is stochastic rather than deterministic, however for E. Coli data obtained in mother machine [32], the coefficient of variation of the volume ratio at division was found to be smaller than 10% [2]. This encourages us to test the validity of our theoretical distributions. We use data from [32], where the size of many independent cell lineages of E. coli has been recorded every minute over 70 generations at three different

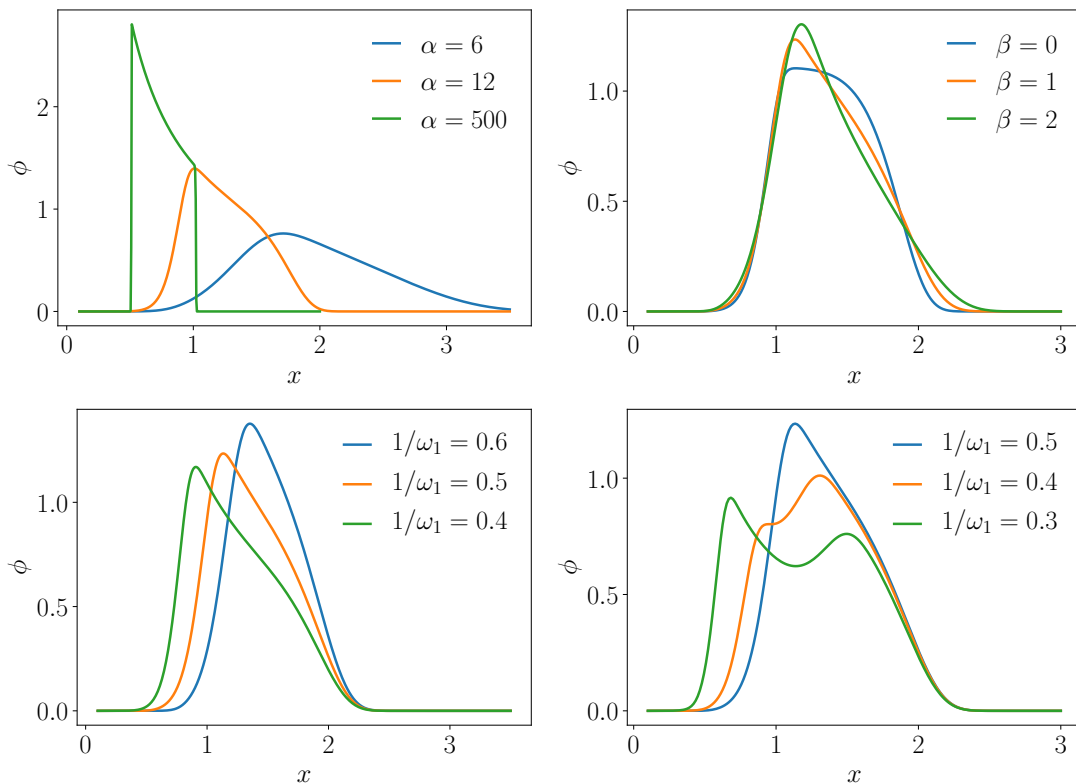


Figure 2. Theoretical lineage distributions for binary fission $m = 2$, for symmetric partitioning on the first row, and asymmetric partitioning on the second row. On the first row, the distribution is computed with eq. (14), with $\beta = 1$ and α varying on the left, and $\alpha = 10$ and β varying on the right. For asymmetric partitioning, the left plot was generated with the smallest daughter tracking protocol (eq. (14) with $m = \omega_1$), and the right plot with the random tracking protocol (eq. (15)). For both plots, we fixed $\alpha = 10$ and $\beta = 1$, and varied the asymmetry ω_1 . For all four plot we fixed $r/\nu = 0.01$.

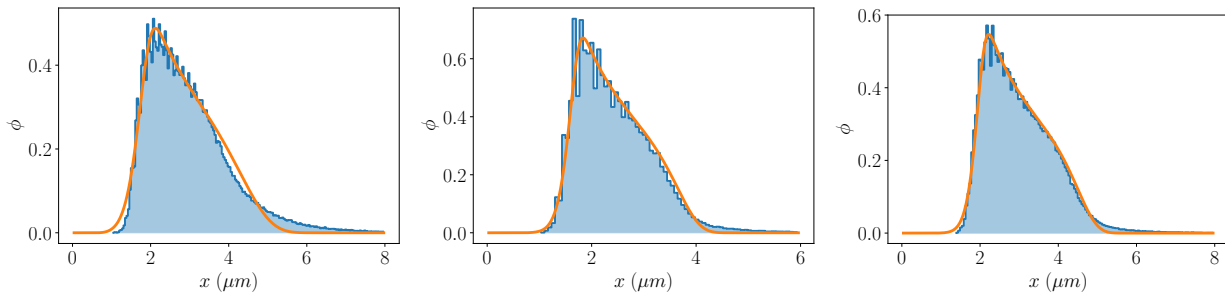


Figure 3. Experimental lineage distributions (blue histograms) for E. Coli data from [32] in three temperature conditions from left to right: 25°C, 27°C and 37°C. The best fits (orange curves) are computed with eq. (14) or eq. (15), and the fitting parameters are given in table I.

temperatures (25°C, 27°C, and 37°C), precisely 65 lineages for 25°C, 54 for 27°C, and 160 for 37°C. We fit the experimental distributions for the three temperatures using the three models: symmetric partitioning, asymmetric partitioning with smaller/larger cell tracking and random tracking. For each temperature, the best fit is shown on fig. 3, and the fitting parameters are given in table I.

First of all, we observe that our model is in very good agreement with experiments at 27°C and 37°C, and that the fit at 25°C is average but fails to capture the slow decay of the right tail. In particular, our results reproduce the three-stages discussed in [2]: fast increase for small cells, slow decay for medium-sized cells, and fast decay for large cells. In the following we analyze the values of the parameters for the condition 27°C and 37°C in particular, given than they provide the best fits to experimental data. Surprisingly, for all temperatures the best fit is given by asymmetric partitioning with smaller-daughter tracking protocol, where the daughter cell which is followed inherits

	25 °C	27 °C	37 °C
Tracking protocol	Smallest daughter	Smallest daughter	Smallest daughter
α	7.89	11.49	13.79
β	1.02	1.26	1.23
$1/\omega_1$	0.40	0.43	0.43
r/ν	4.5×10^{-5}	3.5×10^{-6}	1.8×10^{-7}

Table I. Parameters of the best fits to E. Coli data from [32] shown on fig. 3. In all cases, the best fit was given by the tracking protocol where partitioning is asymmetric and the smallest cell is always followed, given by eq. (14) with $m = \omega_1$.

a fraction $1/\omega_1 = 0.43$ of the mother volume. This value is really close to the value $0.44 - 0.45$ obtained by direct analysis of the sizes at birth and division along the lineages [2]. The strength of the control α tends to increase with temperature, in qualitative agreement with what was found in [2], and the ratio r/ν tends to decrease with temperature. Note that we cannot disentangle the values of r and ν only from the steady-state profile. Finally, the power β in the growth rate is equal to 1.26 for 27 °C at 1.23 for 37 °C, which suggests that in these conditions E. Coli grows slightly faster than exponential for large sizes ($x > 1$), and slightly slower than exponential for small sizes ($x < 1$). This may be linked to the super-exponential growth observed for E. Coli in [33], where the exponential growth rate ν increases during the cell cycle.

To conclude, in spite of the stochasticity in partitioning present in experimental systems, our model for deterministic partitioning gives a very good description of the data for two temperature conditions, and a correct fit for the last temperature. It captures the complexity of the distributions, and the inferred parameters show the same trends as the ones obtained from the model proposed by Jia et al. [2], based on a N -step description of the cell cycle. In contrast to this work, our approach allows growth laws that are more general than exponential, and the dependency of the distributions eq. (14) and eq. (15) on size is more explicit in our model. Also, the present model is simpler in that it involves only one step in the cell cycle. Even though our result produces a fit for the condition 25 °C that is less precise than the one obtained with the N -step model, it performs much better than the N -step model when N is fixed to 1, suggesting that models with N steps may not be necessarily minimal.

IV. ASYMPTOTIC BEHAVIOR FOR GENERAL PARTITIONING KERNEL

In this section, we seek large-size and small-size asymptotic solutions to eq. (5) for general kernels b . We shall see that the tails of the distributions only depend on the behavior of the division rate, growth rate and partitioning kernel at large and small sizes [18]. Therefore, the following results apply to cells obeying more complex growth laws than in the previous section. For example, fission yeasts have been observed to follow piece-wise growing patterns [34, 35], either bi-linear or bi-exponential during the elongation phase. The bacterium *Corynebacterium glutamicum* exhibits asymptotically linear growth [36], unlike most bacteria. In these examples, the growth phases are dictated by the age of the cell, but in size-controlled populations, large (resp. small) cells are on average old (resp. young) cells so that the growth rate at large (resp. small) age is also the growth rate at large (resp. small) size. Moreover, E. Coli has also been shown to deviate from exponential growth for large and small sizes [24].

A. Large size limit

For stochastic partitioning, the large-size population distribution for general growth and division rates behaving as power laws in the large-size limit: $r(x) \underset{x \rightarrow \infty}{\sim} r_\infty x^{\alpha_\infty}$ and $\nu(x) \underset{x \rightarrow \infty}{\sim} \nu_\infty x^{\beta_\infty}$, with $\alpha_\infty - \beta_\infty + 1 > 0$, has been derived by Balagué et al. [18]:

$$\psi(x) \underset{x \rightarrow \infty}{\sim} \nu(x)^{-1} \exp \left[- \int^x dy \frac{\Lambda + r(y)}{\nu(y)} \right] \quad (16)$$

$$\underset{x \rightarrow \infty}{\sim} x^{-\beta_\infty} \exp \left[- \frac{r_\infty}{\nu_\infty} \frac{x^{\alpha_\infty - \beta_\infty + 1}}{\alpha_\infty - \beta_\infty + 1} - \frac{\Lambda}{\nu_\infty} \int^x y^{-\beta_\infty} dy \right]. \quad (17)$$

This result can be understood intuitively as follows: if the distribution is decreasing fast enough in the large-size limit, we can neglect the integral term corresponding to the divisions of larger cells in eq. (3), then the resulting equation is exactly solvable and the solution is eq. (16) [37].

We prove in appendix C 1 and appendix D that the lineage distribution reads

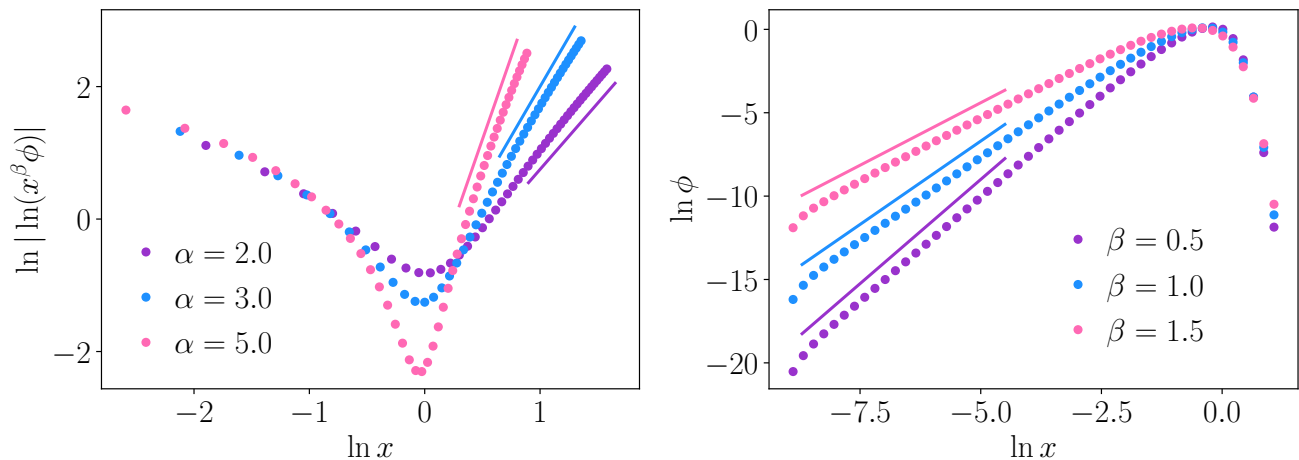


Figure 4. Large and small sizes asymptotic behaviors of the lineage distribution ϕ . For both plots, we fixed $r(x) = x^\alpha$, $\nu(x) = x^\beta$, and $b(x) = x^2(1-x)^2/B(3,3)$ for all x , where $B(x,y)$ is the Beta function. Left: large size limit given by eq. (18) for $\beta = 1$, and for three different values of the strength control α . The slopes $\alpha - \beta + 1 = \alpha$ of the solid lines are, from left to right: 5, 3 and 2. Right: small size limit given by eq. (24) for $\alpha = 5$ and for three different values of β . The slopes $\gamma + 1 - \beta = 3 - \beta$ of the solid lines are, from top to bottom: 1.5, 2 and 2.5.

$$\phi(x) \underset{x \rightarrow \infty}{\sim} x^{-\beta_\infty} \exp \left[-\frac{r_\infty}{\nu_\infty} \frac{x^{\alpha_\infty - \beta_\infty + 1}}{\alpha_\infty - \beta_\infty + 1} \right], \quad (18)$$

which is the population distribution eq. (16) when setting $\Lambda = 0$. The behavior for large sizes is thus independent of the partition kernel b , which implies in particular that it coincides with the large-size behavior for symmetric partitioning obtained by keeping only the first term the series of eq. (14). In order to test this expression, we numerically solve the PBE using a finite difference method with an implicit scheme. Results are shown on fig. 4 left for three different values of the strength of size control $\alpha = 2, 3$ and 5 . In all three cases, the large-size behavior is in very good agreement with the theory.

For cells growing exponentially in the large-size limit, comparing eqs. (17) and (18) leads to the following lineage-population bias:

$$x^{\Lambda/\nu_\infty} \psi(x) \underset{x \rightarrow \infty}{\sim} \phi(x) \quad \text{for } \beta_\infty = 1. \quad (19)$$

If cells grow exponentially with rate $\nu \equiv \nu_\infty$ for all sizes and not only for large-sizes, then we showed in section II B that the population growth rate matches the single cell growth rate $\Lambda = \nu$, so that the lineage-population bias for an arbitrary kernel in the large-size limit is the same as the bias for deterministic symmetric partitioning derived in section II B. This is not surprising since in this limit the behavior does not depend on the kernel.

For arbitrary growth $\beta_\infty \neq 1$, the lineage-population bias is given by:

$$\frac{\psi}{\phi} \underset{x \rightarrow \infty}{\sim} \exp \left[-\frac{\Lambda}{\nu_\infty} \frac{x^{1-\beta_\infty}}{1-\beta_\infty} \right] \quad \text{for } \beta_\infty \neq 1, \quad (20)$$

For any value $\beta_\infty \neq 1$, the right hand side of eq. (20) is a decreasing function of x , showing that large cells are under-represented in the population statistics as compared to the lineage statistics, similarly to what happens for exponential growth.

B. Small size limit

In the following we assume that the growth and division rates asymptotically behave as $\nu(x) \underset{x \rightarrow 0}{\sim} \nu_0 x^{\beta_0}$ and $r(x) \underset{x \rightarrow 0}{\sim} r_0 x^{\alpha_0}$, with $\alpha_0 - \beta_0 + 1 > 0$. We model the partitioning kernel as a power-law $b(x) \underset{x \rightarrow 0}{\sim} b_0 x^{\gamma_0}$ with $\gamma_0 > \beta_0$, which accounts for a broad class of kernels defined on $[0, 1]$, including the Beta distribution commonly used for volume

partitioning [2]. Balagué et al. studied this case and showed that the population distribution was given for small sizes by [18]:

$$\psi(x) \underset{x \rightarrow 0}{\sim} \begin{cases} x^{\gamma_0+1-\beta_0} & \beta_0 < 1 \\ x^{\gamma_0} & \beta_0 \geq 1. \end{cases} \quad (21)$$

In order to understand intuitively the case splitting into two regimes, we give here an argument adapted from the fragmentation theory [38], which is also easily generalizable to the lineage case. We multiply eq. (3) by x^k and integrate over x :

$$r_0(mL_k - 1)M_{k+\alpha_0} = \Lambda M_k - \nu_0 k M_{k+\beta_0-1}. \quad (22)$$

From the power-law behavior of b near 0, we get that not all moments L_k exists: there is a critical $k_c < 0$ under which L_k diverges. First we consider the case $\alpha_0 > 0$. When letting $k \rightarrow k_c^+$, the left hand side of eq. (22) diverges, and so must the moment M of lowest order in the right hand side. When $\beta_0 - 1 \geq 0$, M_k is the moment of lowest order, and must diverge, while $M_{k+\beta_0-1}$ and $M_{k+\alpha_0}$ converges, so that $M_k \propto L_k$, where the proportionality constant is positive. Given the proportionality between the two Mellin-transform, we deduce that ψ is given by the same power law as b : $\psi(x) \underset{x \rightarrow 0}{\sim} x^{\gamma_0}$. On the other hand, when $\beta_0 - 1 < 0$, the moment of lowest order is $M_{k+\beta_0-1}$ and thus $M_{k+\beta_0-1} \propto L_k$, where the proportionality constant is positive, because $k_c < 0$. In that case, Mellin transform properties tell us that $\psi(x) \underset{x \rightarrow 0}{\sim} x^{\gamma_0+1-\beta_0}$. When $\alpha_0 = 0$, the stability condition reads $\beta_0 - 1 < 0$, so that we are in the second case.

The lineage equation on moments is obtained by following the same steps:

$$r_0(L_k - 1)N_{k+\alpha_0} = -\nu_0 k N_{k+\beta_0-1}. \quad (23)$$

The fundamental difference with the population case is the absence of terms in N_k . As a consequence, we obtain $N_{k+\beta_0-1} \propto L_k$ regardless of the value of β_0 , so that:

$$\phi(x) \underset{x \rightarrow 0}{\sim} x^{\gamma_0+1-\beta_0}. \quad (24)$$

This analytical prediction is in perfect agreement with numerical resolutions of the PBE using a finite difference method with an implicit scheme, shown on fig. 4 right, for three different values of $\beta = 0.5, 1$ and 1.5 .

Finally, we obtain the lineage-population bias by comparing eqs. (21) and (24):

$$\psi(x) \underset{x \rightarrow 0}{\sim} \begin{cases} \phi(x) & \beta_0 < 1 \\ x^{\beta_0-1} \phi(x) & \beta_0 \geq 1. \end{cases} \quad (25)$$

When $\beta_0 = 1$, there is no lineage-population bias as predicted in section II B. Indeed, $\psi^{b(x)}(x)$ is equal to $\phi^{2xb(x)}(x)/x \underset{x \rightarrow 0}{\sim} x^{\gamma_0+1}/x = \phi^{b(x)}(x)$, where the factor x and the modified kernel $2xb(x)$ that increases coefficient γ_0 by 1 exactly compensate. Interestingly, there is no bias for any value $\beta_0 < 1$, which, following the discussion of section II B, implies that there is no correlation between size and divisions. Indeed, with deterministic partitioning, the daughter cell inherits half the volume of its mother, so that the only way to reach vanishing sizes it to divide a lot, whereas when all fractions of volume are allowed at division, a cell can also reach small sizes with few divisions if it inherits a small fraction of its mother volume. As a consequence, the correspondence between final size and number of divisions is blurred by the presence of noise in the volume partitioning.

On the other hand, when $\beta_0 \geq 1$, that is for cell growing slower than exponential in the region of small sizes, the lineage-population bias depends on β_0 . Surprisingly, the lineage statistics is biased towards small cells as compared to the population statistics, unlike what we expected from the knowledge of deterministic partitioning. This suggests a correlation between small sizes and small numbers of divisions, that may be explained by the fact that cells that reach very small sizes, because of extremely-asymmetric partitioning, must grow during a very long time before reaching sizes at which they are likely to divide again, and end up with less divisions than average.

C. Validity for the adder model

Until now, we focused on the *sizer* model, where the division rate is only a function of the size x of the cell. Other models of cell size control have been proposed in the literature, such as the *adder* model which accounts for a broad range of experimental data [27, 39]. In this model, the division rate depends on both the size x of the cell

and the added volume since birth $x - x_b$, with x_b the size at birth, in the following way: $r(x, x_b) = \nu(x)\chi(x - x_b)$. This particular choice of division rate ensures that the distribution of volume added between birth and division is independent of the birth volume. In this section, we show that most of the asymptotic results derived above remain valid for the adder model. To do so, let us first write explicitly a PBE for the adder:

$$\partial_t \psi(x, x_b) = -\partial_x [\nu(x)\psi(x, x_b)] - [\Lambda_t + \nu(x)\chi(x - x_b)] \psi(x, x_b) \quad \text{for } x > x_b \quad (26)$$

$$\nu(x_b)\psi(x_b, x_b) = m \int \frac{dx'}{x'} dx'_b b(x_b/x') \nu(x') \chi(x' - x'_b) \psi(x', x'_b), \quad (27)$$

where $\psi(x, x_b)$ is the fraction of cells of size x at time t which were born at size x_b . The lineage equation is obtained from this equation by setting $m = 1$ and $\Lambda_t = 0$ again. Notice already a fundamental difference between this equation and eq. (3): the term accounting for the birth of new cells enters a boundary condition for the adder, because the added volume is reset to 0 at division.

For the large-size limit, a direct integration of the steady-state version of eq. (26) gives

$$\psi(x, x_b) = \psi(x_b, x_b) \frac{\nu(x_b)}{\nu(x)} \exp \left[- \int_{x_b}^x dy \frac{\Lambda}{\nu(y)} + \int_0^{x-x_b} dy \chi(y) \right]. \quad (28)$$

For any given x_b , in the limit where $x \rightarrow +\infty$, we have $x - x_b \sim x$, so that the exponential does not depend on x_b anymore. Thus, the marginal size distribution obeys:

$$\psi(x) \underset{x \rightarrow +\infty}{\sim} C \nu(x)^{-1} \exp \left[- \int^x dy \left(\frac{\Lambda}{\nu(y)} + \chi(y) \right) \right], \quad (29)$$

where $C = \int_0^\infty dx_b \psi(x_b, x_b) \nu(x_b)$ comes from the integration of the joint probability $\psi(x, x_b)$ over x_b . Finally, this large-size behavior is the same as eq. (16) for the sizer, with $r(x) = \nu(x)\chi(x)$. As a consequence, the lineage-population biases in the large-size limit eqs. (19) and (20) remain valid for the adder model.

In the small-size limit, we saw before that the behavior was controlled by the shapes of the division kernel and the growth rate, which are common in the sizer and adder models, so we anticipate that the results are unchanged. To prove it, we still consider $\nu(x) \underset{x \rightarrow 0}{\sim} \nu_0 x^{\beta_0}$ and $b(x) \underset{x \rightarrow 0}{\sim} b_0 x^{\gamma_0}$. Multiplying eq. (26) by x^k and integrating over x and x_b leads after simple manipulations to:

$$\nu_0 (mL_k - 1) \int dx dx_b x^{\beta_0+k} \chi(x - x_b) \psi(x, x_b) = \Lambda M_k - \nu_0 k M_{k+\beta_0-1}, \quad (30)$$

where $M_k = \int_0^\infty dx x^k \psi(x) \equiv \int_0^\infty dx dx_b x^k \psi(x, x_b)$ is the k -th moment of the marginal size distribution $\psi(x)$.

Now we suppose that there is a $\delta_0 \geq 0$ such that $\chi(x) = O(x^{\delta_0})$ when $x \rightarrow 0$, meaning that the division rate per unit volume χ is growing as a power law or slower. In this case, the integral in the left hand side is smaller than $M_{k+\beta_0+\delta_0}$, and thus the integral does not diverge when $M_{k+\beta_0+\delta_0}$ does not diverge. The rest of the proof is the same as for the sizer, where $\beta_0 + \delta_0$ plays the role of α_0 . Finally, the small-size lineage-population biases eq. (25) remain true for the adder model.

Before closing this section, we would like to draw the attention of the reader on the fact that in none of the different lineage-population biases derived in the previous sections does the division rate appear explicitly. In this section we showed that they hold for the adder model, which is a particular choice of two-variable division rate. This observation suggests that these biases could be correct for a much broader class of division rates, possibly involving other variables.

V. NOISY GROWTH

As discussed in the introduction, bacterial size trajectories show some fluctuations around exponential growth. This is illustrated on fig. 5, where we plot a single cell size trajectory using *E. Coli* data from [32]. To account for these fluctuations, we now introduce in-cycle multiplicative noise in the case of exponential growth. To our knowledge, exact solutions to eq. (3) were obtained for deterministic partitioning and only for specific growth rates $\nu(x)$, division rates $r(x)$ and diffusion coefficients $D(x)$. In particular, for asymmetric partitioning, exponential growth $\nu(x) = \nu x$, multiplicative noise $D(x) = Dx^2$ and quadratic division rate $r(x) = rx^2$, the solution is a series of modified Bessel functions, generalizing the Dirichlet series obtained when there is no diffusion, and arising from the quadratic division rate which turns eq. (3) into a modified Bessel equation [40]. Therefore, it seems difficult to generalize this method to more general power law division rates. In this section we seek asymptotic solutions for large sizes and for more general divisions rates $r(x) = rx^\alpha$ and partition kernels.

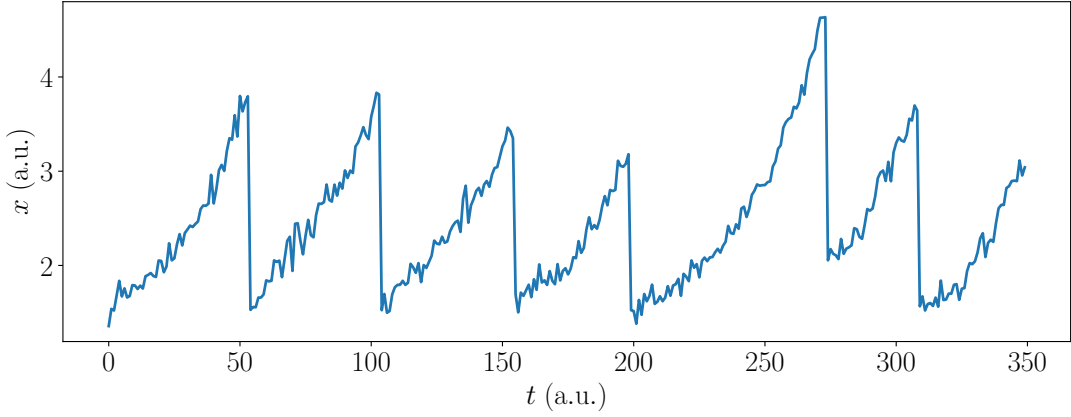


Figure 5. Example of size evolution versus time for a single lineage from [32], in the condition 27°C.

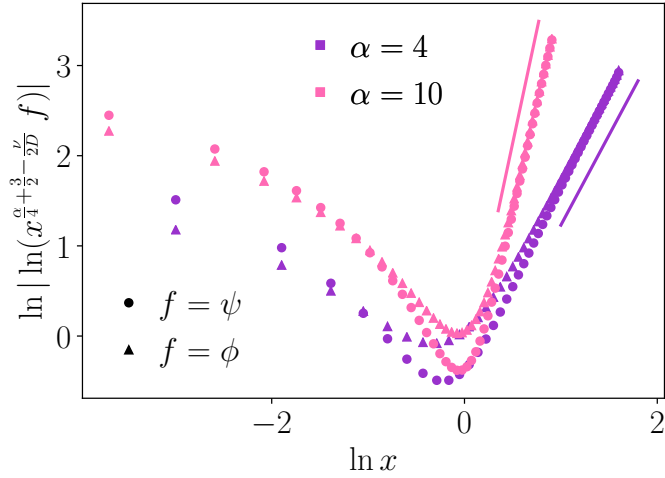


Figure 6. Large size asymptotic behaviors of the lineage and population distributions ϕ and ψ given by eq. (31). We fixed $r(x) = x^\alpha$, $\nu(x) = x$, $D = 0.4$ and $b(x) = x^2(1-x)^2/B(3,3)$ for all x , and show two different values of the strength control α . The slopes $\alpha/2$ of the solid lines are, from left to right: 5 and 2.

We show in appendix C 2 and appendix D that the lineage and population steady state distributions are equivalent in the large size limit and given by

$$\psi(x) \underset{x \rightarrow \infty}{\sim} \phi(x) \underset{x \rightarrow \infty}{\sim} x^{\frac{\nu}{2D} - \frac{3}{2} - \frac{\alpha}{4}} \exp \left[-\frac{2}{\alpha} \sqrt{\frac{r}{D}} x^{\frac{\alpha}{2}} \right]. \quad (31)$$

Just like the case of deterministic growth, the large-size behaviors of ϕ and ψ are independent of the partitioning kernel. In the case $\alpha = 2$, we recover the result obtained in [40] (up to a missing factor \sqrt{x} due to a typo).

We numerically solve the PBE with the diffusive term using a finite difference method, both for the lineage statistics and the population statistics. The scheme is implicit in the first case and hybrid in the second: all terms are implicit except Λ_t , given by eq. (4), which is explicitly computed. Results are shown on fig. 6, for two different values $\alpha = 4$ and $\alpha = 10$ of the size control strength. In both cases, the population and lineage distributions coincide in the large-size limit and align with the theoretical prediction eq. (31).

Unlike the case of deterministic growth discussed in section IV, no lineage-population bias is observed here. This is coherent with eq. (12), where the bias towards smaller cells accounted for by the factor x and the effective growth rate $\nu + 2D$ exactly compensate. Indeed, one easily check from eq. (31) that $\phi_{\nu+2D}(x)/x = \phi_\nu(x)$. Similarly to what happens for small sizes in presence of a stochastic kernel, the lineage-population bias is killed by the presence of multiplicative noise. When there is no noise, only cells that divided few times can reach large sizes, which imposes correlations between the number of divisions and the final size. Here however, this correlation is canceled because the

number of divisions can be balanced by the noisy growth: large cells can come from lineages with numerous divisions if they grew faster on average than the deterministic growth at rate ν .

VI. CONCLUSION

The recent development of mother machine devices revived the interest in the statistical comparison between lineage measurements and population snapshots. The unprecedented amount of single-cell data offers new insights on the way cells regulate their cycle and maintain size homeostasis. It is hence fundamental to quantify the statistics obtained in single-lineage setups and to understand how they differ from classical population snapshot.

To investigate this bias for cell size distributions, we worked on the steady-state population balance equation, separately for the population and lineage levels. We showed that for the special case of exponential growth, the population distribution is proportional to the lineage distribution with modified partitioning kernel and single cell growth rate, divided by the size x . This bias is reminiscent of the correlations between the size and the number of divisions and implies in particular that cells are on average smaller in population than in lineage. For more general power-law growth rates, with deterministic partitioning, we obtained the exact analytical expression for the lineage distribution, which is in good agreement with experimental data on *E. Coli*, despite the slight stochasticity of the partitioning in these data. This expression can then be used to infer the relevant parameters of the model, such as the strength of the size control, the growth rate and the asymmetry of the division. When relaxing the hypothesis of deterministic partitioning, we derived the small and large-size tails for both statistics. We showed that the large-size behavior is independent of the partitioning kernel, and that the lineage-population bias depends only on the growth rate of large cells. In the small size limit, the distributions only depend on the behavior of the partitioning kernel near 0 and of the growth rate of small cells, but is independent of the division rate. Two regimes are observed for the small-size lineage-population bias: for fast-growing small cells it is canceled, while for slow-growing small cells, it explicitly depends on the growth rate of small cells. Importantly, we showed that these asymptotic behaviors remain valid for the adder mechanism, which is increasingly seen as the most relevant model for cell size control. When considering noisy in-cycle growth, the two large-size distributions become equal and explicitly depend on the noise. An important result of this article is the cancellation of the lineage-population bias on cell-size when noise is introduced in the system, either on the growth rate for large sizes, or on the partitioning kernel for small sizes. Indeed, noise kills the correlations between the size and the number of divisions undergone by the cell, thus the selection of lineages with high reproductive success in population has no impact on the size distribution.

This work can be extended in several directions. First, experimental inference suggests a non-trivial behavior of the division rate at large sizes [24], even though the estimation in this region could be unreliable because of the lack of statistics. Therefore, it would be useful to relax the hypothesis of a power-law division rate. Second, we focused on a one-variable model, with the exception of the two-variable adder model, and it would be interesting to investigate more complex models with n variables. For example, modeling cell-to-cell variability in growth imposes to treat the single-cell growth rate ν as a second random variable. Finally, constant-population experiments, such as the dynamics cytometer [41], may not all be well described by a uniform dilution rate, but rather by a dilution rate dependent on size, generation, spatial position, ... In this case, the size distribution obtained would not be the same as in a freely-growing population but would bear the mark of the dilution protocol.

ACKNOWLEDGMENTS

I warmly thank Marie Doumic for her essential help with the mathematical literature, Jérémie Unterberger and David Lacoste for their careful reading of the manuscript, and all these people for useful discussions.

Appendix A: Lineage-population bias for exponentially-growing cells

In this section, we consider the case of exponential growth $\nu(x) = \nu x$ with multiplicative noise $D(x) = Dx^2$, in steady-state so that $\Lambda = \nu$, for which eq. (3) and eq. (5) read:

$$0 = -\nu\partial_x[x\psi(x)] + D\partial_{x^2}[x^2\psi(x)] - [r(x) + \nu]\psi(x) + m \int \frac{dx'}{x'} b(x/x') r(x') \psi(x') \quad (\text{A1})$$

$$0 = -\nu\partial_x[x\phi(x)] + D\partial_{x^2}[x^2\phi(x)] - r(x)\phi(x) + \int \frac{dx'}{x'} b(x/x') r(x') \phi(x'). \quad (\text{A2})$$

We multiply the population equation by x , and recast it for the function $q(x) = x\psi(x)$:

$$0 = -\nu x \partial_x q(x) + Dx \partial_{x^2} [xq(x)] - [r(x) + \nu] q(x) + \int \frac{dx'}{x'} \frac{mx}{x'} b(x/x') r(x') q(x'). \quad (\text{A3})$$

We identify the derivative of a product $-\nu x \partial_x q(x) - \nu q(x) = -\nu \partial_x [xq(x)]$, and show straightforwardly that $Dx \partial_{x^2} [xq(x)] = D \partial_{x^2} [x^2 q(x)] - 2D \partial_x [xq(x)]$, so that the second term is absorbed in the first-order derivative describing exponential growth:

$$0 = -(\nu + 2D) \partial_x [xq(x)] + D \partial_{x^2} [x^2 q(x)] - r(x) q(x) + \int \frac{dx'}{x'} \frac{mx}{x'} b(x/x') r(x') q(x'). \quad (\text{A4})$$

This equation is eq. (A2), obeyed by the lineage distribution ϕ with modified growth rate $\hat{\nu} = \nu + 2D$ and partition kernel $\hat{b}(x) = mx b(x)$, therefore $q(x) \nu^{b(x)}$ is proportional to $\phi_{\nu+2D}^{mx b(x)}$:

$$\phi_{\nu+2D}^{mx b(x)}(x) = K x \psi_{\nu}^{b(x)}(x), \quad (\text{A5})$$

with $K = \left(\int_0^\infty dx x \psi_{\nu}^{b(x)}(x) \right)^{-1}$ a normalization constant. Importantly, \hat{b} is a proper kernel, which is normalized as a consequence of the conservation of volume of the original kernel b : $\int_0^1 dx \hat{b}(x) = m \int_0^1 dx x b(x) = 1$.

Appendix B: Exact lineage solution for deterministic partitioning

In this section, we seek exact solutions to eq. (5) for deterministic single cell growth ($D = 0$) and deterministic volume partitioning, either symmetric or asymmetric.

1. Symmetric partitioning

We follow the method proposed in [28] starting from the steady-state equation:

$$[\nu x^\beta \phi(x)]' = -r x^\alpha \phi(x) + m^{1+\alpha} r x^\alpha \phi(mx), \quad (\text{B1})$$

and we define $Z(x) = x^\beta \phi(x)$, then

$$Z'(x) = \frac{r}{\nu} x^{\alpha-\beta} [-Z(x) + m^{1-\beta+\alpha} Z(mx)]. \quad (\text{B2})$$

We now define $u = r x^{\alpha-\beta+1} / [\nu(\alpha - \beta + 1)]$ and $Y(u) = Z(x)$, so that the equation on Y reads:

$$Y'(u) + Y(u) = m^{1-\beta+\alpha} Y(m^{1-\beta+\alpha} u). \quad (\text{B3})$$

If $1 - \beta + \alpha > 0$, the solution to this equation is [25]:

$$Y(u) = C \sum_{k=0}^{\infty} c_k \exp \left[-m^{k(\alpha-\beta+1)} u \right] \quad (\text{B4})$$

$$c_0 = 1 \quad (\text{B5})$$

$$c_k = \frac{(-1)^k m^{k(\alpha-\beta+1)}}{\prod_{j=1}^k (m^{j(\alpha-\beta+1)} - 1)} \quad k \geq 1. \quad (\text{B6})$$

Reverting to the notation in x with the function ϕ gives

$$\phi(x) = \frac{C}{x^\beta} \sum_{k=0}^{\infty} c_k \exp \left[-m^{k(\alpha-\beta+1)} \frac{r}{\nu} \frac{x^{\alpha-\beta+1}}{\alpha - \beta + 1} \right]. \quad (\text{B7})$$

2. Asymmetric partitioning

For simplicity we consider binary fission ($m = 2$), with asymmetric partitioning: $b(x) = \delta(x - 1/\omega_1)/2 + \delta(x - 1/\omega_2)/2$, where $\omega_1 > \omega_2 > 1$ and $1/\omega_1 + 1/\omega_2 = 1$. Starting from:

$$[\nu x^\beta \phi(x)]' = -rx^\alpha \phi(x) + \frac{rx^\alpha}{2} [\omega_1^{1+\alpha} \phi(\omega_1 x) + \omega_2^{1+\alpha} \phi(\omega_2 x)] , \quad (\text{B8})$$

and making the same two changes of variables as for the symmetrical case, the equation reads

$$Y'(u) + Y(u) = \frac{1}{2} [\Omega_1 Y(\Omega_1 u) + \Omega_2 Y(\Omega_2 u)] , \quad (\text{B9})$$

where we defined $\Omega_i = \omega_i^{1-\beta+\alpha}$ for $i \in \{1, 2\}$. If $1 - \beta + \alpha > 0$, the solution to this equation is [42]:

$$Y(u) = C \sum_{k=0}^{\infty} \sum_{l=0}^{\infty} c_{k,l} \exp[-\Omega_1^k \Omega_2^l u] \quad (\text{B10})$$

$$c_{0,0} = 1 \quad (\text{B11})$$

$$c_{k,0} = \frac{(-1)^k \Omega_1^k}{2^k \prod_{j=1}^k (\Omega_1^j - 1)} \quad (\text{B12})$$

$$c_{0,l} = \frac{(-1)^l \Omega_2^l}{2^l \prod_{j=1}^l (\Omega_2^j - 1)} \quad (\text{B13})$$

$$c_{k,l} = \frac{\Omega_1 c_{k-1,l} + \Omega_2 c_{k,l-1}}{2 - 2\Omega_1^k \Omega_2^l} . \quad (\text{B14})$$

Reverting to the original notations gives

$$\phi(x) = \frac{C}{x^\beta} \sum_{k=0}^{\infty} \sum_{l=0}^{\infty} c_{k,l} \exp \left[-\omega_1^{k(\alpha-\beta+1)} \omega_2^{l(\alpha-\beta+1)} \frac{r}{\nu} \frac{x^{\alpha-\beta+1}}{\alpha - \beta + 1} \right] . \quad (\text{B15})$$

Appendix C: Asymptotic lineage distribution for stochastic partitioning

In the following subsections, we drop the subscript ∞ for simplicity, since only the large-size limit is investigated, and we make two general comments. First, when the limit $k \rightarrow +\infty$ (resp. $k \rightarrow -\infty$) is considered, corresponding to the large- x (resp. small- x) limit, the integrals of the type $\int_0^\infty dx x^k f(x)$ are dominated by the behavior of the function f as $x \rightarrow \infty$ (resp. as $x \rightarrow 0$). Therefore, when for example $r(x) \underset{x \rightarrow \infty}{\sim} rx^\alpha$, we write $\int_0^\infty dx x^k r(x) \phi(x) \underset{k \rightarrow \infty}{\sim} \int_0^\infty dx x^k r x^\alpha \phi(x) = r N_{\alpha+k}$. Second, the following transformation is used to isolate the moments L of the kernel b [38]:

$$\int_0^\infty dx x^k \int_x^\infty dy b(x/y) y^{\alpha-1} \phi(y) \quad (\text{C1})$$

$$= \int_0^\infty dy y^\alpha \phi(y) \int_0^y dx x^k b(x/y) \quad (\text{C2})$$

$$= \int_0^\infty dy y^{k+\alpha} \phi(y) \int_0^1 du u^k b(u) \quad (\text{C3})$$

$$= N_{\alpha+k} L_k , \quad (\text{C4})$$

where we went from the second to the third line with the change of variable $u = x/y$.

1. Deterministic growth

We first consider the case of deterministic growth ($D = 0$) for an arbitrary growth rate with power β , and follow the method proposed in [38] for fragmentation processes. We multiply eq. (5) by $x^{k-\beta+1}$ and integrate over x , to

recast the PBE as a recursion relation on the moments of the distribution:

$$N_{k+\alpha-\beta+1} \underset{k \rightarrow \infty}{\sim} \frac{\nu}{r} \frac{k-\beta+1}{1-L_{k-\beta+1}} N_k. \quad (\text{C5})$$

For simplicity we define $\rho = \alpha - \beta + 1 > 0$, and n such that $k = n\rho$, leading to

$$N_{(n+1)\rho} \underset{n \rightarrow \infty}{\sim} \frac{\nu}{r} \frac{n\rho - \beta + 1}{1 - L_{n\rho - \beta + 1}} N_{n\rho}. \quad (\text{C6})$$

Iterating this relation leads to the general term:

$$N_{n\rho} \underset{n \rightarrow \infty}{\sim} N_\rho \left(\frac{\nu}{r}\right)^{n-1} \prod_{j=1}^{n-1} \frac{j\rho - \beta + 1}{1 - L_{j\rho - \beta + 1}}. \quad (\text{C7})$$

We compute the numerator as

$$\prod_{j=1}^{n-1} (j\rho - \beta + 1) = \rho^{n-1} (n-1)! \prod_{j=1}^{n-1} \left(1 - \frac{\beta-1}{j\rho}\right) \quad (\text{C8})$$

$$\underset{n \rightarrow \infty}{\sim} \rho^{n-1} (n-1)! (n-1)^{\frac{1-\beta}{\rho}}, \quad (\text{C9})$$

where we used that $\prod_{j=1}^n \left(1 - \frac{a}{j}\right) \sim n^{-a}$ as $n \rightarrow \infty$.

We now show that the moments $L_{j\rho - \beta + 1}$ of the partition kernel can be neglected in this limit. We consider a power-law partition kernel $b(x) = b_1(1-x)^\gamma$ in the limit $x \rightarrow 1$, but the argument can be made more general.

$$L_k \underset{k \rightarrow \infty}{\sim} b_1 \int_0^1 dx x^k (1-x)^\gamma \quad (\text{C10})$$

$$\underset{k \rightarrow \infty}{\sim} k^{-(\gamma+1)}, \quad (\text{C11})$$

where we recognize the Beta function $B(k+1, \gamma+1) = \int_0^1 dy y^k (1-y)^\gamma$, whose asymptotic behavior when only one of the two parameters tends to infinity (here k) is given by: $B(k+1, \gamma+1) \underset{k \rightarrow \infty}{\sim} \Gamma(\gamma+1) k^{-(\gamma+1)}$. The product in the denominator of eq. (C7) is therefore given by

$$\ln \prod_{j=1}^{n-1} (1 - L_{j\rho - \beta + 1}) = \sum_{j=1}^{n-1} \ln(1 - L_{j\rho - \beta + 1}) \quad (\text{C12})$$

$$\underset{n \rightarrow \infty}{\sim} - \sum_{j=1}^{n-1} (j\rho - \beta + 1)^{-(\gamma+1)}, \quad (\text{C13})$$

where the second line is obtained by a first-order expansion of the natural logarithm. Finally, since $\gamma > 0$, this series is converging when $n \rightarrow \infty$.

The general term then reads

$$N_{n\rho} \underset{n \rightarrow \infty}{\sim} \left(\frac{\rho\nu}{r}\right)^{n-1} (n-1)! (n-1)^{\frac{1-\beta}{\rho}}. \quad (\text{C14})$$

We next use Stirling approximation: $n! \underset{n \rightarrow \infty}{\sim} \sqrt{2\pi n} (n/e)^n$, switch back to $k = n\rho$ and replace ρ :

$$N_k \underset{k \rightarrow \infty}{\sim} \left(\frac{\nu k}{r e}\right)^{\frac{k}{\alpha-\beta+1}} k^{\frac{1-\beta}{\alpha-\beta+1} - \frac{1}{2}}. \quad (\text{C15})$$

The inverse Mellin transform of this moment is obtained in appendix D.

2. Stochastic growth

We examine the case of exponential growth $\nu(x) = \nu x$ with multiplicative noise $D(x) = Dx^2$. Following the same steps as for the deterministic growth, multiply eq. (3) and eq. (5) by x^k and integrate over x :

$$M_{k+\alpha} \underset{k \rightarrow \infty}{\sim} \frac{1}{r} \frac{\nu(k-1) + Dk(k-1)}{1 - mL_k} M_k \quad (\text{C16})$$

$$N_{k+\alpha} \underset{k \rightarrow \infty}{\sim} \frac{1}{r} \frac{\nu k + Dk(k-1)}{1 - L_k} N_k. \quad (\text{C17})$$

As for the deterministic case, the moments L_k are negligible for large k , so that the moments $M_{k+\alpha}$ and $N_{k+\alpha}$ differ only by their numerators. We conduct the calculations for the lineage distribution first and then show why the difference in the numerators does not affect the general moment.

We define n such that $k = n\alpha$, and iterate the relation to obtain the general term:

$$N_{n\alpha} \underset{n \rightarrow \infty}{\sim} N_\alpha \left(\frac{1}{r}\right)^{n-1} \prod_{j=1}^{n-1} \frac{\nu j\alpha + Dj\alpha(j\alpha - 1)}{1 - L_{j\alpha}}. \quad (\text{C18})$$

The numerator is computed as:

$$\prod_{j=1}^{n-1} [\nu j\alpha + Dj\alpha(j\alpha - 1)] = (\alpha^2 D)^{n-1} (n-1)!^2 \prod_{j=1}^{n-1} \left(1 - \frac{D - \nu}{j\alpha D}\right) \quad (\text{C19})$$

$$\underset{n \rightarrow \infty}{\sim} (\alpha^2 D)^{n-1} (n-1)!^2 (n-1)^{\frac{\nu-D}{\alpha D}}. \quad (\text{C20})$$

The Stirling approximation: $n!^2 \underset{n \rightarrow \infty}{\sim} 2\pi n(n/e)^{2n}$ is used to obtain

$$N_{n\alpha} \underset{n \rightarrow \infty}{\sim} \left(\frac{\alpha^2 D}{r}\right)^{n-1} \left(\frac{n-1}{e}\right)^{2(n-1)} (n-1)^{\frac{\nu-D}{\alpha D} + 1}. \quad (\text{C21})$$

Switching back to $k = n\alpha$ leads to:

$$N_k \underset{k \rightarrow \infty}{\sim} \left(\sqrt{\frac{D}{r}} \frac{k}{e}\right)^{\frac{2k}{\alpha}} k^{\frac{2}{\alpha} \frac{\nu-D}{2D} - 1}. \quad (\text{C22})$$

The inverse Mellin transform of this moment is obtained in appendix D.

The numerator of the general moments $M_{n\alpha}$ is given by

$$\prod_{j=1}^{n-1} [\nu(j\alpha - 1) + Dj\alpha(j\alpha - 1)] = (\alpha^2 D)^{n-1} (n-1)!^2 \prod_{j=1}^{n-1} \left(1 - \frac{1}{j\alpha}\right) \prod_{j=1}^{n-1} \left(1 + \frac{\nu}{j\alpha D}\right) \quad (\text{C23})$$

$$\underset{n \rightarrow \infty}{\sim} (\alpha^2 D)^{n-1} (n-1)!^2 (n-1)^{-\frac{1}{\alpha}} (n-1)^{\frac{\nu}{\alpha D}}, \quad (\text{C24})$$

which is identical to eq. (C20), so that the moment M_k is equal to N_k given by eq. (C22), and leads to the same distribution for large sizes.

Appendix D: Mellin transform of polynomial-exponential distribution

For a distribution y characterized by its large x behavior:

$$y(x) \underset{x \rightarrow \infty}{\sim} x^{\eta - \lambda(\mu - 1/2) - 1} \exp\left[-\frac{x^\lambda}{\lambda\omega}\right], \quad (\text{D1})$$

the moments of large order read

$$M_k \underset{k \rightarrow \infty}{\sim} \int_0^\infty dx x^{k + \eta - \lambda(\mu - 1/2) - 1} e^{-\frac{x^\lambda}{\lambda\omega}} \quad (\text{D2})$$

$$\sim \lambda^{-1} (\lambda\omega)^{(k+\eta)/\lambda - \mu + 1/2} \int_0^\infty dt t^{(k+\eta)/\lambda - \mu - 1/2} e^{-t}, \quad (\text{D3})$$

where we went from the first to the second line using the change of variable $t = x^\lambda/\lambda\omega$. We recognize the function $\Gamma(z) = \int_0^\infty dt t^{z-1}e^{-t}$ in the second line with $z = (k + \eta)/\lambda - \mu + 1/2$, and we use the Stirling approximation: $\Gamma(z + 1) \underset{z \rightarrow \infty}{\sim} \sqrt{2\pi z} \left(\frac{z}{e}\right)^z$. Finally, the Mellin transform reads:

$$M_k \underset{k \rightarrow \infty}{\sim} \lambda^{-\frac{3}{2}} (\lambda\omega)^{(k+\eta)/\lambda - \mu + 1/2} \sqrt{2\pi(k + \eta - \lambda(\mu + 1/2))} \left(\frac{k + \eta - \lambda(\mu + 1/2)}{\lambda e}\right)^{\frac{k+\eta}{\lambda} - \mu - 1/2} \quad (\text{D4})$$

$$\sim \left(\frac{k\omega}{e}\right)^{\frac{k}{\lambda}} k^{\frac{\eta}{\lambda} - \mu}. \quad (\text{D5})$$

-
- [1] Wang P, Robert L, Pelletier J, Dang WL, Taddei F, Wright A, Jun S. 2010 Robust Growth of Escherichia coli. *Curr. Biol.* **20**, 1099–1103.
- [2] Jia C, Singh A, Grima R. 2021 Cell size distribution of lineage data: Analytic results and parameter inference. *iScience* **24**, 102220.
- [3] Jia C, Singh A, Grima R. 2022 Characterizing non-exponential growth and bimodal cell size distributions in fission yeast: An analytical approach. *PLoS Comput. Biol.* **18**, e1009793.
- [4] Levien E, GrandPre T, Amir A. 2020 Large Deviation Principle Linking Lineage Statistics to Fitness in Microbial Populations. *Phys. Rev. Lett.* **125**, 048102.
- [5] Genthon A, Lacoste D. 2020 Fluctuation relations and fitness landscapes of growing cell populations. *Sci. Rep.* **10**, 11889.
- [6] Pigolotti S. 2021 Generalized Euler-Lotka equation for correlated cell divisions. *Phys. Rev. E* **103**, L060402.
- [7] Powell EO. 1956 Growth Rate and Generation Time of Bacteria, with Special Reference to Continuous Culture. *J. Gen. Microbiol.* **15**, 492–511.
- [8] Levien E, Kondev J, Amir A. 2020 The interplay of phenotypic variability and fitness in finite microbial populations. *J. R. Soc. Interface* **17**, 20190827.
- [9] Nakashima S, Sughiyama Y, Kobayashi T.J. 2020 Lineage EM algorithm for inferring latent states from cellular lineage trees. *Bioinformatics* **36**, 2829–2838.
- [10] Nozoe T, Kussell E, Wakamoto Y. 2017 Inferring fitness landscapes and selection on phenotypic states from single-cell genealogical data. *PLoS Genet.* **13**, e1006653.
- [11] Thomas P. 2017 Making sense of snapshot data: ergodic principle for clonal cell populations. *J. R. Soc. Interface* **14**, 20170467.
- [12] Thomas P. 2018 Analysis of Cell Size Homeostasis at the Single-Cell and Population Level. *Front. Phys.* **6**, 64.
- [13] Genthon A, Lacoste D. 2021 Universal constraints on selection strength in lineage trees. *Phys. Rev. Research* **3**, 023187.
- [14] García-García R, Genthon A, Lacoste D. 2019 Linking lineage and population observables in biological branching processes. *Phys. Rev. E* **99**, 042413.
- [15] Totis N, Nieto C, Kuper A, Vargas-García C, Singh A, Waldherr S. 2021 A Population-Based Approach to Study the Effects of Growth and Division Rates on the Dynamics of Cell Size Statistics. *IEEE Control Syst. Lett.* **5**, 725–730.
- [16] Michel P. 2006 Existence of a solution to the cell division eigenproblem. *Math. Models Methods Appl. Sci.* **16**, 1125–1153.
- [17] Doumic Jauffret M, Gabriel P. 2010 Eigenelements of a general aggregation-fragmentation model. *Math. Models Methods Appl. Sci.* **20**, 757–783.
- [18] Balagué D, Cañizo J, Gabriel P. 2013 Fine asymptotics of profiles and relaxation to equilibrium for growth-fragmentation equations with variable drift rates. *Kinet. Relat. Models* **6**, 219–243.
- [19] Doumic M, Hoffmann M, Krell N, Robert L. 2015 Statistical estimation of a growth-fragmentation model observed on a genealogical tree. *Bernoulli* **21**, 1760–1799.
- [20] Olivier A. 2017 How does variability in cell aging and growth rates influence the Malthus parameter?. *Kinet. Relat. Mod.* **10**, 481–512.
- [21] Lin J, Amir A. 2020 From single-cell variability to population growth. *Phys. Rev. E* **101**, 012401.
- [22] Kiviet DJ, Nghe P, Walker N, Boulineau S, Sunderlikova V, Tans SJ. 2014 Stochasticity of metabolism and growth at the single-cell level. *Nature* **514**, 376–379.
- [23] Basse B, Wake GC, Wall DJN. 2004 On a cell-growth model for plankton. *Math. Med. Biol.* **21**, 49–61.
- [24] Robert L, Hoffmann M, Krell N, Aymerich S, Robert J, Doumic M. 2014 Division in Escherichia coli is triggered by a size-sensing rather than a timing mechanism. *BMC Biol.* **12**, 17.
- [25] Hall AJ, Wake GC. 1989 A functional differential equation arising in modelling of cell growth. *J. Aust. Math. Soc. Series B, Appl. Math* **30**, 424–435.
- [26] Nieto C, Arias-Castro J, Sánchez C, Vargas-García C, Pedraza JM. 2020 Unification of cell division control strategies through continuous rate models. *Phys. Rev. E* **101**, 022401.
- [27] Taheri-Araghi S, Bradde S, Sauls J, Hill N, Levin P, Paulsson J, Vergassola M, Jun S. 2015 Cell-Size Control and Homeostasis in Bacteria. *Curr. Biol.* **25**, 385–391.
- [28] Hall AJ, Wake GC. 1990 Functional differential equations determining steady size distributions for populations of cells growing exponentially. *J. Aust. Math. Soc. Series B, Appl. Math* **31**, 434–453.

- [29] Alonso AA, Molina I, Theodoropoulos C. 2014 Modeling Bacterial Population Growth from Stochastic Single-Cell Dynamics. *Appl. Environ. Microbiol.* **80**, 5241–5253.
- [30] Doumic M, Hoffmann M. 2021 Individual and population approaches for calibrating division rates in population dynamics: Application to the bacterial cell cycle. *arXiv:2108.13155 [math, stat]*.
- [31] Zaidi AA, van Brunt B. 2021 Asymmetrical cell division with exponential growth. *ANZIAM J.* **63**, 70–83.
- [32] Tanouchi Y, Pai A, Park H, Huang S, Buchler NE, You L. 2017 Long-term growth data of Escherichia coli at a single-cell level. *Sci. Data* **4**, 170036.
- [33] Kar P, Tiruvadi-Krishnan S, Männik J, Männik J, Amir A. 2021 Distinguishing different modes of growth using single-cell data. *eLife* **10**, e72565.
- [34] Horváth A, Rácz-Mónus A, Buchwald P, Sveiczler A. 2013 Cell length growth in fission yeast: an analysis of its bilinear character and the nature of its rate change transition. *FEMS Yeast Res* **13**, 635–649.
- [35] Pesti B, Nagy Z, Papp L, Sipiczki M, Sveiczler A. 2021 Cell Length Growth in the Fission Yeast Cell Cycle: Is It (Bi)linear or (Bi)exponential?. *Processes* **9**, 1533.
- [36] Messelink JJ, Meyer F, Bramkamp M, Broedersz CP. 2021 Single-cell growth inference of Corynebacterium glutamicum reveals asymptotically linear growth. *eLife* **10**, e70106.
- [37] Friedlander T, Brenner N. 2008 Cellular Properties and Population Asymptotics in the Population Balance Equation. *Phys. Rev. Lett.* **101**, 018104.
- [38] Cheng Z, Redner S. 1988 Scaling Theory of Fragmentation. *Phys. Rev. Lett.* **60**, 2450–2453.
- [39] Jun S, Si F, Pugatch R, Scott M. 2018 Fundamental principles in bacterial physiology—history, recent progress, and the future with focus on cell size control: a review. *Rep. Prog. Phys.* **81**, 056601.
- [40] Zaidi AA, van Brunt B, Wake GC. 2016 Probability density function solutions to a Bessel type pantograph equation. *Applicable Analysis* **95**, 2565–2577.
- [41] Hashimoto M, Nozoe T, Nakaoka H, Okura R, Akiyoshi S, Kaneko K, Kussell E, Wakamoto Y. 2016 Noise-driven growth rate gain in clonal cellular populations. *Proc. Natl. Acad. Sci. U.S.A.* **113**, 3251–3256.
- [42] Suebcharoen T, van Brunt B, Wake GC. 2011 Asymmetric cell division in a size-structured growth model. *Differ. Integral Equ.* **24**, 787–799.